A STATISTICAL EXAMINATION OF THE SENSE RECONSTRUCTION VIA AN ISOMORPHISM REPRESENTATION

By

Iain P. Bruce

A Thesis submitted to the Faculty of the Graduate School,
Marquette University,
in Partial Fulfillment of the Requirements for
the Degree of Master of Science

Milwaukee, Wisconsin

April 2011

ABSTRACT

A STATISTICAL EXAMINATION OF THE SENSE RECONSTRUCTION VIA AN ISOMORPHISM REPRESENTATION

Iain P. Bruce

Marquette University

In MRI, the parallel acquisition of sub-sampled spatial frequencies from an array of multiple receiver coils has become a common means of reducing data acquisition time. SENSitivity Encoding (SENSE) is a popular parallel image reconstruction model that uses a complex-valued least squares estimation process to unfold aliased images. In this manuscript, the linear mathematical framework derived in Rowe et al. [J Neurosci Meth 159(2007) 361–369] is built upon to perform image reconstruction with sub-sampled data acquired from multiple receiver coils, where the SENSE model is represented as a real-valued isomorphism. A statistical analysis is performed of the various image reconstruction operators utilized in the SENSE model, with an emphasis placed on the effects of each operator on voxel means, variances, and correlations. It is shown that despite the attractiveness of models that unfold the aliased images from sub-sampled data, there is an artificial correlation induced between reconstructed voxels from the different folds of aliased images. As such, the mathematical framework outlined in this manuscript could be further developed to provide a means of accounting for this unavoidable correlation induced by image reconstruction operators.

ACKNOWLEDGEMENTS

Iain P. Bruce

I would like to portray my most sincere gratitude to my Advisor, Dr. Rowe, for the invaluable time and support he has provided in completing this work. I would also like to thank both Andrew Hahn and Muge Karaman for their contributions in our research discussion sessions. Their advice proved most useful on a variety of occasions allowing me to further understand the field of fMRI. Finally, I would like to thank the Wehr Foundation, as this work was funded by the Computational Sciences Summer Research Program (CSSRP) at Marquette University in the Department of Mathematics, Statistics, and Computer Science.

TABLE OF CONTENTS

1. INTRODUCTION

The discovery that the spatial information of an object can be encoded in the resonance spectrum by a magnetic field gradient [1,2] is the fundamental basis for image formation in magnetic resonance imaging (MRI). Although several mathematical basis sets (Fourier, Hadamard, Wavelet, Singular Value Decomposition) have been used to encode the spatial information of an object, Fourier encoding is by far the most prevalent. The complex-valued spatial frequencies of a real-valued object, Fourier encoded by magnetic field gradients, are not measured instantaneously and thus need to be measured individually in a serial fashion. It can take on the order of one to two seconds to measure the required spatial frequencies to form a volume of images at resolutions as low as 64×64 voxels. As such, significant effort has been put forth on many fronts, including the measurement of spatial frequencies with multiple receiver coils, in parallel, to decrease image acquisition time [3]

A variety of parallel acquisition methods, such as SENSitivity Encoding (SENSE), use multiple receiver coils to sub-sample spatial frequency points in parallel, and later combine the multiple coil images into a single image [4]. SENSE is a popular parallel image reconstruction technique as it is very flexible in terms of the choice of coil layout, and the reduction in scan time achieved by sub-sampling the data relaxes the requirements placed on studies such as breath holding in cardiac imaging [5]. Although sub-sampling data in parallel can dramatically reduce the time involved in acquiring data, it conversely results in an increase in image reconstruction time and difficulty

SENSE utilizes a linear regression method based on a complex-valued regression coefficient estimation process with transposes replaced by Hermitians to obtain complex-valued images. An unavoidable consequence of the SENSE model that to the best of our knowledge has not been discussed is that the “unfolding” process involved in generating a full field-of-view

(FOV) image from sub-sampled data induces a correlation between the aliased voxels from each "fold." This correlation can in turn be amplified if pre-processing operators such as image smoothing are utilized, resulting in regions of voxels correlated with the corresponding regions from other folds. As this correlation is set in place before any analysis has been performed on the image itself, it is obvious that any correlations deduced from the data could be very misleading after image reconstruction.

In this manuscript, we utilize the mathematical framework derived in [6] to represent the operators involved in image reconstruction in a linear matrix-multiplication fashion. The AMMUST (A Mathematical Model for Understanding the STatistical effects) framework for analyzing reconstruction and pre-processing operators described in [7] is expanded upon to allow for sub-sampled data from multiple receiver coils to be used in the SENSE reconstruction model. The operators involved in SENSE image reconstruction are used to illustrate the correlation induced between the aliased voxels of sub-sampled data, as well as the amplification of said correlation when pre-processing operations such as image smoothing are applied. The correlations induced by the SENSE operators are theoretically illustrated on 96×96 noiseless phantom data as well as on experimental phantom and human subject fMRI data. A real-valued isomorphism representation of the complex-valued coil covariance matrix is estimated from an experimental time series of scans of a spherical Phantom, and an experimental time series of resting state scans with a human subject.

2. THEORY

2.1 Image Reconstruction Operators

The AMMUST framework in [7] generalized the mathematical formalism of image reconstruction in [6] using a Cartesian linear image reconstruction. The current work expands

upon this Cartesian framework in a manner that accounts for the acquisition of sub-sampled data from an array of receiver coils. This allows for the examination of statistical properties of parallel image reconstruction.

The ability to perform a complex-valued inverse Fourier reconstruction by means of a real-valued isomorphism, a real-valued process for performing a complex-valued operation, as derived in [6], paves the way for a statistical analysis of the operations commonly undertaken by parallel data acquisition and reconstruction techniques such as SENSE. The real-valued isomorphism allows a reconstructed complex-valued image, in vector form, y, to be represented as the product of an inverse Fourier reconstruction operator, Ω, with the observed complex-valued k-space spatial frequencies in vector form, f, as:

$$y = \Omega f \ . \tag{1}$$

It can be shown that the above equation holds true for any linear reconstruction operator, Ω, however, the inverse Fourier transform is utilized throughout the remainder of this study. If F_C is a $p_y \times p_x$ matrix of two-dimensional complex-valued spatial frequencies, comprised of the sum of a true noiseless complex-valued spatial frequency matrix F_{0C}, and a matrix of complex-valued measurement error E_C,

$$F_C = F_{0C} + E_C \,, \tag{2}$$

then the vector of observed k-space spatial frequencies, f, in Eq. (1) are formed by stacking the $p_x p_y$ real spatial frequencies on top of the $p_x p_y$ imaginary spatial frequencies

$$f = vec(\mathrm{Re}(F_C^T), \mathrm{Im}(F_C^T)) \,,$$

where $vec(\cdot)$ is a vectorization operator that stacks the columns of its matrix argument, Re denotes the real part, and Im denotes the imaginary part. This vectorization thus concatenates the rows of

the real and imaginary matrices into separate vectors, which are in turn concatenated into a single vector, f, that is of dimension $2p_xp_y\times1$. As with F_C, f is the sum of a vector of true noiseless (complex-valued) spatial frequencies, f_0, and a vector of (complex-valued) measurement error, ε. Similarly to the observed k-space data, if the complex-valued reconstructed image is of dimensions $p_y\times p_x$, then the reconstructed image vector will consist of p_xp_y real reconstructed image values stacked above p_xp_y imaginary reconstructed image values, resulting in a reconstructed image vector y of dimensions $2p_xp_y\times1$.

Given that the complex-valued reconstructed magnetic resonance image is an inverse Fourier transform of the measured complex-valued spatial frequencies,

$$Y(q_x\Delta x, q_y\Delta y) = \sum_{q_y=-m}^{m-1}\sum_{q_x=-n}^{n-1} F(p_x\Delta x, p_y\Delta y)\exp\left(i2\pi\left(\frac{p_xq_x}{2n}+\frac{p_yq_y}{2m}\right)\right)$$

consider the inverse Fourier transform matrices in the x and y directions

$$\Omega_{xC} = \Omega_{xR} + i\Omega_{xI},\quad \Omega_{yC} = \Omega_{yR} + i\Omega_{yI}$$

where Ω_{xR} and Ω_{xI} denote the real and imaginary matrix parts respectively in the x direction [6]. The jk^{th} element of Ω_{xC} can be expressed as

$$(\Omega_{xC})_{jk} = \exp\left(\frac{i2\pi}{p_x}+\left(j-\left(\frac{p_x}{2}+1\right)\right)*\left(k-\left(\frac{p_x}{2}+1\right)\right)\right),$$

where j and k vary from 1 to p_x [7]. A similar inverse Fourier matrix can be expressed for Ω_{yC} that is of dimension p_y. Both Ω_{xC} and Ω_{yC} can be adjusted to account for intra-acquisition decay and magnetic field inhomogeneities acquired in the k-space signal [7,8] if T_2^* or ΔB maps can be obtained. The complex-valued inverse Fourier transformation of F_C can be written as

$$Y_C = \Omega_{yC}F_C\Omega_{xC} \tag{3}$$

The inverse Fourier transformation of spatial frequencies used in Eq. (3) is illustrated in Fig. 1. Fig. 1c shows the *k*-space spatial frequency matrix F_C, that is pre-multiplied by the inverse Fourier transform matrix Ω_{yC}, in Fig. 1b, and post-multiplied by the inverse Fourier transform matrix Ω_{xC}, in Fig. 1d, resulting in the complex-valued image space image in Fig. 1a.

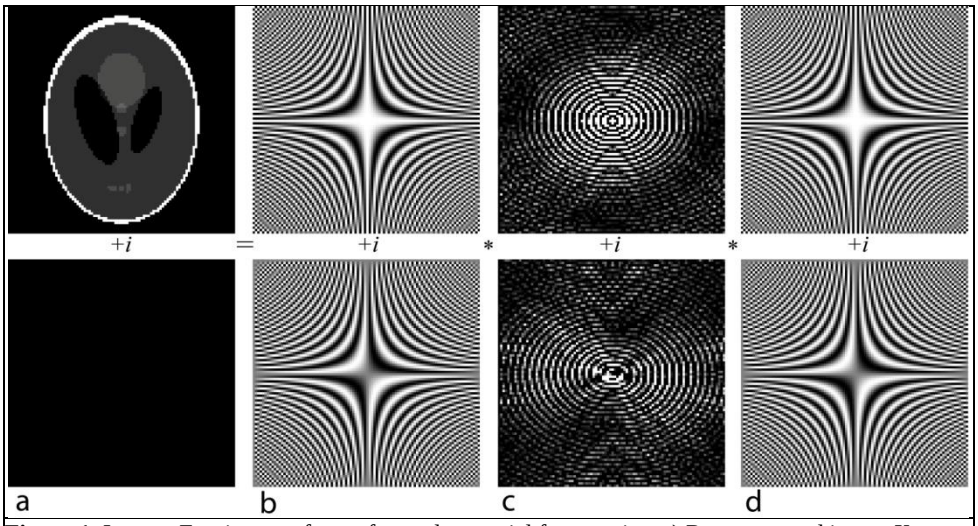

Figure 1. Inverse Fourier transform of complex spatial frequencies. a) Reconstructed image Y_C b) Ω_{yC} inverse Fourier transform matrices c) spatial frequencies F_C d) Ω_{xC} inverse Fourier transform matrices

For simplicity in representation and examination of reconstruction, it can be shown that the pre- and post- multiplication of inverse Fourier matrices can be combined into a single reconstruction matrix

$$\Omega = \begin{bmatrix} \Omega_R & -\Omega_I \\ \Omega_I & \Omega_R \end{bmatrix}$$

where the real and imaginary components are derived using the Kronecker product, $\otimes$, as

$$\Omega_R = [(\Omega_{yR} \otimes \Omega_{xR}) - (\Omega_{yI} \otimes \Omega_{xI})], \quad \Omega_I = [(\Omega_{yR} \otimes \Omega_{xI}) + (\Omega_{yI} \otimes \Omega_{xR})].$$

The Kronecker product operator multiplies every element of its first matrix argument by its entire second matrix argument. Pre-multiplying the spatial frequency vector, *f*, by the combined inverse Fourier transform matrix, Ω, the reconstructed image in Eq. (1) can be expressed as

$$\begin{pmatrix} y_R \\ y_I \end{pmatrix} = \begin{bmatrix} \Omega_R & -\Omega_I \\ \Omega_I & \Omega_R \end{bmatrix} \begin{pmatrix} f_{0R} + \varepsilon_R \\ f_{0I} + \varepsilon_I \end{pmatrix}. \quad (4)$$

While the spatial frequency vector, *f*, may be comprised of real and imaginary values, the application of the Fourier transform operator in Eq. (4) results in a covariance between the real measurements, imaginary measurements, and a covariance between the real and imaginary (real/imaginary). Eq. (4) lays the groundwork for the AMMUST framework in [7] that is necessary to analyze the operations involved in image reconstruction for fully-sampled data from a single receiver coil. With mere inverse Fourier image reconstruction, the covariance matrix of the reconstructed image is modified by the reconstruction operator Ω as

$$\mathrm{cov}(y) = \Omega \Gamma \Omega^T \quad (5)$$

where Γ is the covariance matrix of the observed vector of *k*-space data. It is important to note that although Γ might only have a real and imaginary covariance structure, the resultant covariance in Eq. (5) will also have a covariance between the real and imaginary as well as a covariance between the imaginary and real (imaginary/real). With additional operators to be described later, such as permutations, image smoothing, and the SENSE unfolding operator, the reconstruction in Eq. (1) becomes

$$y = Of\ , \quad (6)$$

where *O* signifies the series of linear operators expressed as matrix multiplications applied throughout the image reconstruction process. Just as in Eq. (5), the covariance matrix induced through a series of operators, *O*, can be calculated by

$$\Sigma = \mathrm{cov}(y) = O \Gamma O^T\ . \quad (7)$$

Similar to the structure of the spatial frequencies in Eq. (2), Γ is the covariance of the spatial frequencies, f, which is comprised of a mean signal vector, f_0, and a noise vector, ε. The covariance matrices Γ and Σ contain real by real, imaginary by imaginary and real by imaginary covariances. The vectors f_0 and ε contain real and imaginary spatial frequencies and noise elements. The derivation outlined in the Appendices of [7] allows for the covariance structure of the square of the magnitude-only data (magnitude-squared data) to be derived from the covariance matrix Σ in Eq. (7) assuming normality. Magnitude-squared data is considered in the analysis of the covariance and correlation induced by operators involved in image reconstruction because an analytical solution exists for the linear framework in this study, while magnitude-only data is not considered as magnitude operations are not linear in nature. It can be shown that the correlation of magnitude-squared data is asymptotically equivalent to the correlation of magnitude-only data, and thus will be used along with complex-valued data to observe properties of real, imaginary, and real/imaginary correlation structures.

2.2 Parallel Imaging of Sub-sampled Data

Although Eq. (4) is expressed for data from a single receiver coil that acquires a full FOV, it can be generalized to reconstruct sub-sampled data from an array of multiple receiver coils. Traditionally, under-sampling data occurs by skipping lines of *k*-space in the Phase Encoding (PE) direction, although the framework and principle can be applied for any direction, with any scheme in which lines of data are sub-sampled. In this Cartesian framework, the subscript y denotes the PE direction (i.e. top-bottom), while the subscript x denotes the frequency encode direction (i.e. left-right). For an acceleration factor (also commonly known as a reduction factor), A, a receiver coil would only acquire every A^{th} line of *k*-space in the PE direction. Thus, a sub-sampled matrix of spatial frequencies F_C would be of dimensions $(p_y/A)\times p_x$. This sub-sampled data set is vectorized in exactly the same fashion as the full dataset in Eq. (2), where the

vector of observed sub-sampled *k*-space spatial frequencies, *f*, in Eq. (1) is formed by stacking the $p_x(p_y/A)$ real spatial frequencies on top of the $p_x(p_y/A)$ imaginary spatial frequencies. In order to utilize the inverse Fourier reconstruction operator, Ω, it is necessary for Ω_{yC} to include the correct dimension to transform the reduced FOV.

As will be illustrated, when implementing a SENSE image reconstruction of sub-sampled data from multiple receiver coils, it is necessary to select an acceleration factor that is less than the total number of coils in the array, otherwise it results in a sensitivity matrix that is not sufficiently defined. As such, in order to implement the process of sub-sampling data with an acceleration factor greater than A=1, it is necessary to have more than one receiver coil.

Consider an array of N_C receiver coils, each of which acquires a $(p_y/A)\times p_x$ sub-sampled spatial frequency matrix. The vector of spatial frequencies, *f*, will be comprised of N_C vectors of the vectorized real spatial frequencies from each coil stacked above the imaginary component of spatial frequencies from the corresponding coils. In this form, the vectorized spatial frequencies from each coil can be inverse Fourier transformed via the Ω operator, as in Eq. (4), by carrying out the Kronecker product $I_{N_C}\otimes\Omega$.

With a Kronecker product, every element of I_{N_C} is multiplied by the entire matrix Ω, generating a block diagonal inverse Fourier reconstruction operator for a reduced FOV image reconstruction of each coil image

$$y_{coil} = \left(I_{N_C} \otimes \Omega \right) f \ , \tag{8}$$

where

$$y_{coil} = vec(\mathrm{Re}({y_{coil}}^T), \mathrm{Im}({y_{coil}}^T))$$

is a vector concatenating the sub-vectors *coil* = [1,2,..,N_C] of the real reconstructed coil images stacked upon the corresponding imaginary reconstructed coil images. The consequence of skipping lines in *k*-space is an aliased image. This effect is illustrated in Fig. 2 where a magnitude image of a modified Shepp-Logan phantom (top left) represented by its spatial frequencies (top right) is reduced by a factor of *A*=3 (bottom right) in the phase encoding direction (top-bottom) to produce an aliased image (bottom left).

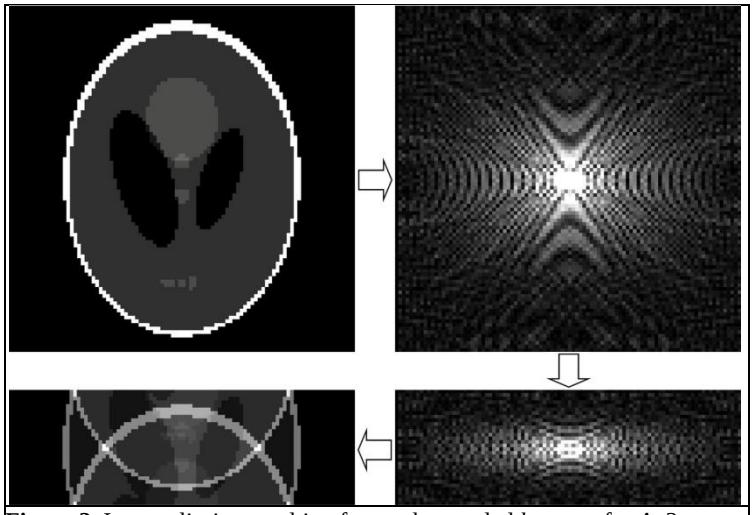

Figure 2. Image aliasing resulting from sub-sampled *k*-space, for *A*=3

The aliased images from the N_C receiver coils are combined and un-aliased, or "unfolded," via the SENSE unfolding matrix in conjunction with the coil covariance matrix. The combination of these images first requires a permutation that rearranges the vector y_{coil}, that was ordered by coil image, to now being ordered by voxel. The result of such a permutation is another vector containing the same elements but the elements are rearranged with the N_C real image values stacked upon N_C imaginary image values for each aliased voxel in the N_C coil images. This reordering operation can be undertaken by pre-multiplying the product $(I_{N_C} \otimes \Omega)f$ by a complex permutation matrix P_C, resulting in a vector of elements ordered by reduced FOV folded image space voxel values

$$a = P_C \left(I_{N_C} \otimes \Omega \right) f \, . \tag{9}$$

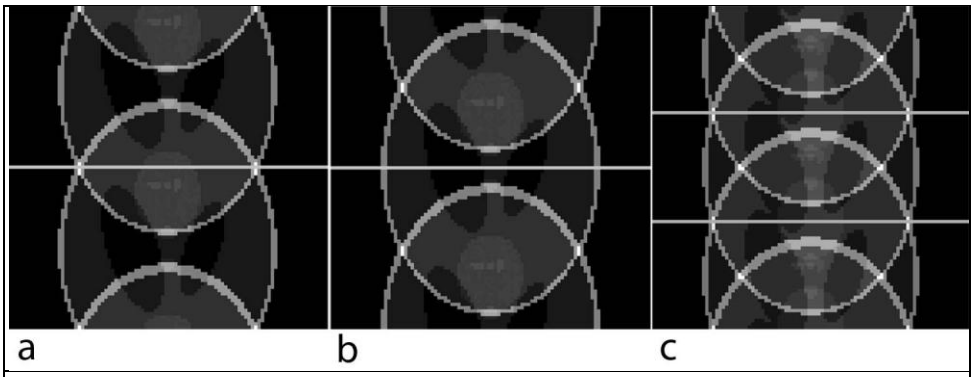

Figure 3. Fourier transform shift permutation required for even acceleration factors. a) *A*=2 IFT without Shift b) *A*=2 IFT with Shift c) *A*=3 IFT without Shift

A permutation matrix such as P_C is a matrix of zeros and ones that when pre-multiplying a vector, the resulting vector contains the same elements but in a different order. In addition to the complex permutation applied in Eq. (9), for even acceleration factors it may be necessary to apply a second permutation that performs a Fourier transform shift. For an acceleration factor of *A*=2, the center line of *k*-space will be in the center of the aliased image, and thus an "unfolding" will lead to an image that does not fulfill the Nyquist criteria. This ultimately results in the reconstructed image in Fig. 3a that appears to be off center. However, if a Fourier transform shift is applied to the aliased images after Fourier reconstruction, then the center line of *k*-space will align itself with the edge of a fold. Consequently, the folds themselves will align their edges with the edge of the full FOV, as illustrated in Fig. 3b. This is not, however, an issue for odd acceleration factors, as illustrated in Fig. 3c for an acceleration factor of *A*=3. This is because although the center-line of *k*-space lies within the center of a fold, when unfolding the aliased images, the edges of the folds are aligned with the edge of the full FOV as well. As such, a Fourier transform shift permutation, P_S, pre-multiplies the complex permutation in Eq. (9) whenever an even acceleration factor, *A*, is selected

$$a = P_S P_C \left(I_{N_C} \otimes \Omega \right) f \,. \tag{10}$$

2.3 SENSE

Within the SENSE model with N_C receiver coils, voxel j contains a complex-valued vector $a_{jC} = a_{jR} + i\, a_{jI}$ of N_C voxel measurements from the sub-sampled spatial frequencies, that are derived by

$$a_{jC} = S_{jC} v_{jC} + \varepsilon_{jC} . \tag{11}$$

In Eq. (11), $S_{jC} = S_{jR} + iS_{jI}$ is derived from the fully sampled complex-valued coil image sensitivity matrix, $v_{jC} = v_{jR} + iv_{jI}$ is the complex-valued true scalar voxel, and $\varepsilon_{jC} = \varepsilon_{jR} + i\varepsilon_{jI}$ is the complex-valued additive measurement noise. For the estimation of each of the aliased voxel values, the matrix S_{jC} is of dimension $N_C \times A$, a_{jC}, and ε_{jC} are of dimension $N_C \times 1$, while v_{jC} is a vector of length A denoting values of each of the A aliased voxel values. It is generally assumed that the complex-valued measurement noise, ε_{jC}, is derived from the complex-valued normal distribution [9] given by

$$f(\varepsilon_{jC}) = (2\pi)^{-N_C} \left|\Psi_C\right|^{-1/2} \exp\left(-\frac{1}{2} \varepsilon_{jC}^H \Psi_C^{-1} \varepsilon_{jC} \right)$$

where $\Psi_C = \Psi_R + i\Psi_I$ is the complex-valued coil covariance matrix and H denotes the Hermetian or conjugate transpose. With this error structure, the complex-valued vector of sub-sampled spatial frequencies, a_{jC}, can be shown with a change of variables to have a complex-valued normal distribution

$$f(a_{jC}) = (2\pi)^{-N_C} \left|\Psi_C\right|^{-1/2} \exp\left[-\frac{1}{2} (a_{jC} - S_{jC} v_{jC})^H \Psi_C^{-1} (a_{jC} - S_{jC} v_{jC}) \right]. \tag{12}$$

The least-squares estimate of the complex-valued true scalar voxel values, as used for the SENSE estimate of the un-aliased single combined voxel values is

$$v_{jC} = (S_{jC}^H \Psi_C^{-1} S_{jC})^{-1} S_{jC}^H \Psi_C^{-1} a_{jC} . \quad (13)$$

Alternatively Eq. (11) can be expressed as a real-valued isomorphism

$$a_j = S_j v_j + \varepsilon_j \quad (14)$$

where $a_j = (a_{jR}^T, a_{jI}^T)^T$ is a vector of N_C real measurements stacked upon a vector of N_C imaginary measurements, $\varepsilon_j = (\varepsilon_{jR}^T, \varepsilon_{jI}^T)^T$ is a vector of the N_C real parts of the complex-valued additive noise stacked upon a vector of the N_C imaginary parts. The vector of the complex-valued scalar voxel values $v_j = (v_{jR}^T, v_{jI}^T)^T$ is also comprised of the real part stacked upon the imaginary part. The unfolded scalar voxel values, v, are derived from an array of fully sampled spatial frequencies from each coil

$$S_j = \begin{bmatrix} S_{jR} & -S_{jI} \\ S_{jI} & S_{jR} \end{bmatrix} \quad (15)$$

where S_{jR} and S_{jI} are the real and imaginary vectors of coil image sensitivities for the voxel of interest j in the folded image.

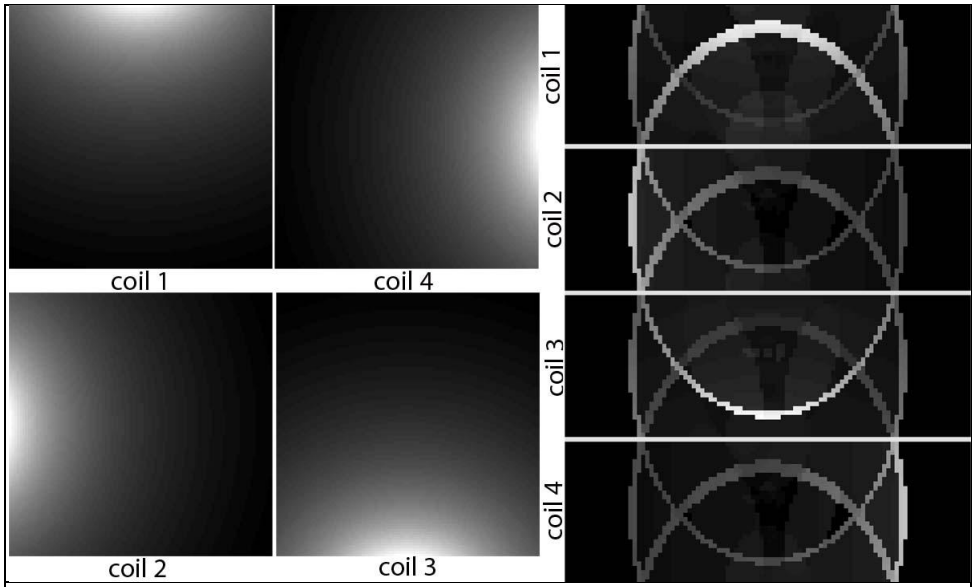

Figure 4. Sensitivity maps and their corresponding aliased coil images for an array of N_C=4 coils.

The aliased surface coil images, from the reception field sensitivities of the N_C=4 receiver coils in Fig. 4a, are illustrated in Fig. 4b.

Using the isomorphism in Eq. (14), the complex-valued multivariate normal distribution can be expressed as the $2N_C \times 1$ multivariate normal distribution of coil measurements in Eq. (12) by

$$f(a_j) = (2\pi)^{-N_C} \left|\Psi\right|^{-1/2} \exp\left[-\frac{1}{2}(a_j - S_j v_j)^T \Psi^{-1}(a_j - S_j v_j) \right].$$

As the additive measurement noise, derived from the complex-valued normal distribution

$$\varepsilon_{jC} \sim CN\left(0, \Psi_C\right)$$

provides the correlation between the coils in the SENSE model, when represented as a real-valued isomorphism,

$$\varepsilon_j \sim N\left(0, \begin{bmatrix} \Psi_R & -\Psi_I \\ \Psi_I & \Psi_R \end{bmatrix}\right),$$

the real-valued isomorphism complex coil covariance matrix, as used in the SENSE model, is expressed as

$$\Psi = \begin{bmatrix} \Psi_R & -\Psi_I \\ \Psi_I & \Psi_R \end{bmatrix}. \tag{16}$$

What Eq. (16) implies is that the real/imaginary covariance between coils is the negative of the imaginary/real, making the overall coil covariance structure skew-symmetric. In many studies, Ψ_C (and hence Ψ) is treated as an real-valued identity matrix, however, it will be shown in the Experimental Illustration that this is far from the correct structure when the coil covariance is estimated from real data.

Provided with the real-valued isomorphism representation of the complex-valued coil sensitivities matrix as in Eq. (15) and the real-valued isomorphism representation of the complex-valued coil covariance matrix as in Eq. (16), the SENSE estimator for the un-aliased single combined voxel values in Eq. (13) can be equivalently expressed as a real-valued isomorphism

$$\begin{bmatrix} v_{jR} \\ v_{jI} \end{bmatrix} = \left(\begin{bmatrix} S_{jR} & -S_{jI} \\ S_{jI} & S_{jR} \end{bmatrix}^T \begin{bmatrix} \Psi_R & -\Psi_I \\ \Psi_I & \Psi_R \end{bmatrix}^{-1} \begin{bmatrix} S_{jR} & -S_{jI} \\ S_{jI} & S_{jR} \end{bmatrix} \right)^{-1} \begin{bmatrix} S_{jR} & -S_{jI} \\ S_{jI} & S_{jR} \end{bmatrix}^T \begin{bmatrix} \Psi_R & -\Psi_I \\ \Psi_I & \Psi_R \end{bmatrix}^{-1} \begin{bmatrix} a_{jR} \\ a_{jI} \end{bmatrix}$$

or

$$v_j = (S_j^T \Psi^{-1} S_j)^{-1} S_j^T \Psi^{-1} a_j \tag{17}$$

where S_j is of dimension $2N_C \times 2A$, Ψ is of dimension $2N_C \times 2N_C$, and the vector of voxel measurements a_j is of dimension $2N_C \times 1$. Thus, the isomorphism in Eq. (17) yields an image space vector, v_j, of dimension $2A \times 1$ that is comprised of the A real voxel values stacked upon the A imaginary voxel values. These A-values correspond to the A folds that are formed via under-sampling the data in k-space by a factor of A. It can be shown that the real and imaginary parts of the estimated complex-valued un-aliased single combined image voxel value in Eq. (13) is mathematically equivalent to the estimated real and imaginary isomorphism vector of un-aliased single combined image voxel value in Eq. (17).

In order to carry out the SENSE isomorphism using the linear framework in Eqs. (8-10), Eq. (17) is rewritten as

$$v = Ua$$

where the SENSE unfolding matrix U is block diagonal with j^{th} block for voxel j

$$U_j = (S_j^T \Psi^{-1} S_j)^{-1} S_j^T \Psi^{-1}$$

and

$$a = P_S P_C \left(I_{N_C} \otimes \Omega \right) f \, .$$

The SENSE estimation in Eq. (17) can be expressed as a single operator to unfold all aliased voxels in the reduced images at once. Provided with the fully sampled coil sensitivities, S_j, a coil sensitivity matrix, S, can be constructed by placing the $2N_C \times 2A$ coil sensitivities corresponding to each aliased voxel, j, where j varies from voxel 1 to voxel rp, along the diagonal of a block diagonal matrix. With a covariance between voxels of Υ, the covariance structure of the k-space data, acquired from independent receiver coils, with a coil covariance of Ψ is defined to be

$$\Gamma = \frac{p_x p_y}{A} \left(\Psi \otimes \Upsilon \right) \tag{18}$$

where $p_x(p_y/A)$ is a scalar multiple produced by the Fourier transformation from image space to k-space. In order to reconstruct all voxels at once with a voxel covariance Υ, the SENSE unfolding operators is expressed as

$$U = \left(S^T \left(\Upsilon \otimes \Psi \right)^{-1} S \right) S^T \left(\Upsilon \otimes \Psi \right)^{-1} \tag{19}$$

where the order of Ψ and Υ in Eq. (18) are switched in the Kronecker product in Eq. (19) because the data being unfolded is ordered by voxel rather than by coil. In the literature, the general practice is to use an identity covariance between voxels in the SENSE model. Thus, if Υ is assumed to be an identity matrix with rp diagonal elements, the SENSE unfolding operator becomes

$$U = \left(S^T \left(I_{rp} \otimes \Psi \right)^{-1} S \right) S^T \left(I_{rp} \otimes \Psi \right)^{-1} .$$

When U is applied as an operator, it will perform the real-valued estimation in Eq. (17), "unfolding" the N_C real and N_C imaginary voxel values in all rp aliased voxels from the N_C coils into A real and A imaginary voxel values for each of A folds

$$v = UP_S P_C \left(I_{N_C} \otimes \Omega \right) f \, .$$

It is then necessary to apply a third permutation, P_U, that reorders the un-aliased real and imaginary image values in y from being ordered by voxel to being ordered by fold, and then from being ordered by fold to ordered by row, resulting in a vector of all real image values stacked upon all imaginary image values

$$y = P_U UP_S P_C \left(I_{NC} \otimes \Omega \right) f \tag{20}$$

or

$$y = P_U v \, .$$

Additional operators for pre-processing in k-space, O_K, and image space processing, O_I, can be incorporated into Eq. (20) as

$$y = O_I P_U UP_S P_C \left(I_{N_C} \otimes \Omega O_K \right) f \, .$$

These operators are treated as identity in this study unless specified otherwise. The operators used to reconstruct the acquired k-space data in Eq. (20) can be combined into a single operator as

$$O = O_I P_U UP_S P_C \left(I_{N_C} \otimes \Omega O_K \right). \tag{21}$$

From this collection of operators, the modified covariance by the reconstruction and pre-processing operators themselves can be evaluated as

$$\Sigma_{SE} = \mathrm{cov}(y) = O\Gamma O^T .$$

where Γ is the covariance matrix of the acquired *k*-space data. In the analysis of the statistical properties induced by the reconstruction operators, Γ is assumed to be identity, and thus any Σ that is not proportional to an identity matrix is an induced covariance between voxels. As such, the induced covariance between voxels from the SENSE reconstruction operators is

$$\begin{aligned}\Sigma_{SE} &= OO^T \\ &= O_I P_U U P_S P_C \left(I_{N_C} \otimes \Omega O_K\right)\left(I_{N_C} \otimes \Omega O_K\right)^T P_C{}^T P_S{}^T U^T P_U{}^T O_I{}^T .\end{aligned}$$

Thus for any of the operators in Eq. (21), such as the unfolding permutation P_U, the covariance induced by that operator of choice is evaluated as

$$\Sigma_{P_U} = P_U O O^T P_U{}^T$$

where $O = UP_SP_C(I_{N_C} \otimes \Omega O_K)$ denotes the collection of all operators pre-multiplied by P_U in Eq. (21). Therefore, if the operators in O are all orthogonal, Σ will be either an identity matrix, or a scaled identity matrix.

For an arbitrary operator (or collection of operators) O, assuming spatial frequencies with an identity covariance between voxels, the correlation induced between voxels is derived by

$$\mathrm{corr}(O) = D_O{}^{-1/2} O O^T D_O{}^{-1/2} \qquad (22)$$

where D_O=diag(Σ) is a diagonal matrix of the variances from the diagonal of the covariance matrix Σ=OO^T and the -1/2 superscript denotes that the diagonal elements are square rooted and inverted. The real-valued isomorphism correlation matrix produced by Eq. (22) can be partitioned into quadrants as

$$\text{corr}(\Sigma) = \begin{bmatrix} RR & RI \\ IR & II \end{bmatrix},$$

where any row, *j*, of the each quadrant denotes the correlation between voxel *j* and all other voxels in the reconstructed image for the respective complex denomination. The correlation about voxel *j* can be generated by dividing the j^{th} row of each quadrant in corr(Σ) into p_x vectors of $1 \times p_y$, each of which denotes a column of the reconstructed image, stacking the row vectors into a matrix, and finally transposing.

2.3.1 Selection of the Acceleration Factor *A*

It is necessary for N_C to be greater than the acceleration factor *A* in order to perform the inversion in the complex-valued weighted least squares estimation in the SENSE model [10]. An increase in acceleration factor, *A*, is marked by a decrease in the number of signal values received by each coil by a factor of A. Transitioning from *k*-space to image-space via inverse Fourier transform, the image-space variance is equivalent to the original *k*-space variance divided by the *k*-space dimensions. Thus, a reduction in *k*-space dimensions, by a factor of *A*, effectively scales the standard deviation in image space by a factor of $(A)^{1/2}$. Therefore, the ratio between the signal-to-noise ratio (SNR) of a full FOV acquisition and a reduced FOV in a voxel *j* is expressed as

$$SNR_j^{red} = \frac{SNR_j^{full}}{g_j \sqrt{A}}$$

where

$$g_j = \frac{SNR_j^{full}}{SNR_j^{red} \sqrt{A}} = \sqrt{\left[\left(S^H \Psi^{-1} S\right)^{-1}\right]_{j,j} \left[\left(S^H \Psi^{-1} S\right)\right]_{j,j}}$$

is the geometry factor (*g*-factor). The *g*-factor is commonly used as a means of assessing the geometry of the array of receiver coils. The *g*-factor essentially determines the level of noise amplification that results from the reconstruction process, and describes how well aliased voxels will be unfolded given the choice of coil geometry. It depends heavily on how different the N_C coil sensitivities are in any aliased voxel *j*, but is also influenced by the covariance between receiver coils. Ideally, an array of independent receiver coils with sensitivity profiles that do not overlap and do not decrease in strength with distance from the coil (i.e. similar to that of a pie with slices of equal size and constant throughout), would result in a *g*-factor of 1 in every voxel. However, this coil arrangement is very difficult to achieve, and thus the coil sensitivity profiles usually have considerable overlap. The *g*-factor is improved by increasing the number of receiver coils, and maintaining an acceleration factor, *A*, that is somewhat less than N_C [10]. Doing so results in an over-determined system of equations, improving the numerical condition of the matrix inversion utilized in the SENSE least-squares estimation of voxel values in Eq. 17.

3. Theoretical Illustration

Within this illustration, data is generated from a true noiseless Shepp-Logan phantom with a theoretical coil covariance consistent with that of real data between N_C=4 receiver coils. Recall from Eq. (6) that a full FOV vectorized image in image space with real image values stacked upon imaginary image values, *y*, is reconstructed through a variety of operators, *O*, that pre-multiply a vector, *f*, containing a series of N_C sub-sampled vectors of real *k*-space data stacked upon corresponding vectors of imaginary *k*-space data. Starting with a real-valued isomorphism representation of a true noiseless real-valued Shepp-Logan phantom, *y*, the vector of *k*-space data, *f*, can be derived from Eq. (6) with a least squares estimation by

$$f = (O^T O)^{-1} O^T y.$$

Under the assumption that there is an identity covariance structure between voxels in Eq. (19), the result of this procedure is a vector of sub-sampled *k*-space data from N_C receiver coils that exhibits an appropriate theoretical covariance between each of the coils, consistent with that of real data.

To illustration the covariance and correlation induced by the individual operators, operators will be generated to reconstruct a 9×9 image with an acceleration factor of A=3, while a 96×96 modified Shepp-Logan phantom image, scaled to have a maximum value of 50, is used to illustrate the correlation induced by operators on the individual voxels themselves. As complex data is gathered in both real and imaginary channels, an appropriate choice of coil covariance, in terms of a real-valued isomorphism matrix, is

$$\Psi_{coil} = \begin{bmatrix} \Psi_{RR} & \Psi_{RI} \\ \Psi_{RI}^{\ T} & \Psi_{II} \end{bmatrix},$$

where $\Psi_{RR}=\Psi_R$ is the real coil covariance, $\Psi_{II}=\Psi_I$ is the imaginary coil covariance, and $\Psi_{RI}=\Psi_{IR}^{\ T}$ is the covariance between the real and imaginary channels. In this illustration, the real and imaginary coil covariances were chosen to be circular Markovian, resembling the covariance estimated from experimental data as

$$\Psi_R = \Psi_I = \begin{bmatrix} 1 & 0.33 & 0.11 & 0.33 \\ 0.33 & 1 & 0.33 & 0.11 \\ 0.11 & 0.33 & 1 & 0.33 \\ 0.33 & 0.11 & 0.33 & 1 \end{bmatrix}.$$

A non-symmetric covariance was chosen between the real and imaginary channels to observe the effects of the skew-symmetric coil covariance used in the SENSE model in Eq. (16).

$$\Psi_{RI} = \begin{bmatrix} 0.000 & -0.11 & -0.07 & -0.11 \\ 0.263 & 0.000 & -0.11 & -0.07 \\ 0.417 & 0.263 & 0.000 & -0.11 \\ 0.263 & 0.417 & 0.263 & 0.000 \end{bmatrix}.$$

Reconstructed mean magnitude and phase images are illustrated in Fig. 5. It can be seen in Fig. 5a and 5c that there appears to be some aliasing in both the magnitude and phase reconstructed images. This is most likely a result of the skew-symmetric coil covariance structure assumed by the SENSE model.

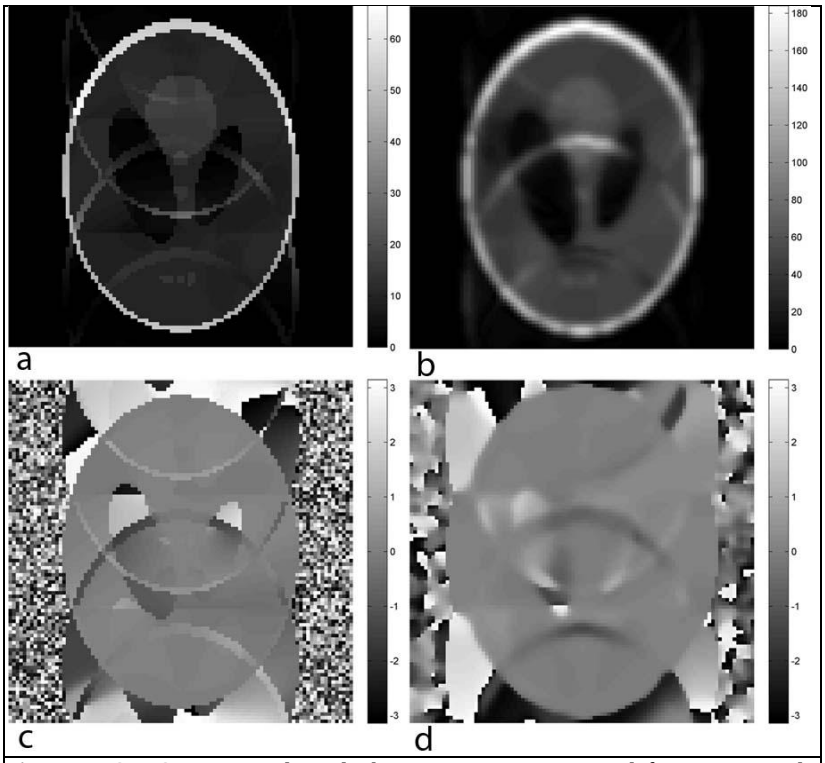

Figure 5. SENSE Magnitude and Phase Images reconstructed from N_C=4 coils, reduced in the PE direction for an acceleration factor of A=3 with and without smoothing. a) unsmoothed magnitude b) unsmoothed phase c) smoothed magnitude d) smoothed phase.

As it is common practice to perform image smoothing after reconstruction, a Gaussian kernel, $O_I = S_m$, with a full width at half maximum of three voxels was applied in image space after reconstruction

$$y = S_m P_U U P_S P_C \left(I_{N_C} \otimes \Omega O_K \right) f \,.$$

The SENSE operators for reconstructing *k*-space data are thus

$$O = S_m P_U U P_S P_C \left(I_{N_C} \otimes \Omega O_K \right)$$

where $O_K = I$.

As outlined in Appendix A, in order for the variance of the data to remain unchanged, the magnitude is scaled by the inverse of the square root of the sum of squares of the elements within the Gaussian kernel. For the chosen Gaussian kernel in this illustration, with a FWHM of three voxels, the ratio of the smoothed and un-smoothed mean images is 4.516. One can see this increase in magnitude when comparing the un-smoothed magnitude image in Fig 5a to those that are smoothed in Fig. 5b. The ghosting in the SENSE magnitude and phase imaged in Fig. 5b and Fig. 5d appears to remain unaffected when the data is smoothed. However, note that the aliasing itself in the SENSE magnitude in Fig. 5a is smoothed, and thus becomes spread out to neighboring voxels in Fig. 5b.

Each of the operators in the SENSE model along with the covariance and correlation induced by each operator are presented in Fig. 6 for a 9×9 reconstruction with an acceleration factor of A=3 and N_C=4 receiver coils. The unfolding permutation, shift permutation, complex permutation, and inverse Fourier transform operators are illustrated in Figs. 6a, 6b, 6c, and 6d respectively. As all three permutations simply rearrange the order of the data that they pre-multiply, they do not individually induce any covariance, i.e. $P_U P_U^{\mathrm{T}}=P_S P_S^{\mathrm{T}}=P_C P_C^{\mathrm{T}}=I$, and in turn induce an identity correlation between voxels. As the inverse Fourier transform reconstruction operator, Ω, is orthogonal, $\Omega\Omega^{\mathrm{T}}=1/(p_x p_y/A)I$, there is no correlation is induced by image reconstruction, as illustrated in Fig. 6f, but the variances are reduced by a factor of $1/(p_x p_y/A)I$, as shown in Fig. 6e. The SENSE unfolding operator, U, resembles the block diagonal matrix, as illustrated in Fig. 6g. Each block unfolds the N_C real and N_C imaginary image values from the N_C coils into A real and A imaginary image values corresponding to the A folds. The voxel measurements from each of the N_C coils are covariant by the choice of the coil covariance matrix, Ψ. Therefore, as each block along the diagonal of U represents a $2N_C$ to $2A$ mapping of image values, there is a resulting block diagonal covariance between the corresponding voxels from

each of the *A* folds in Fig. 6h. Consequently, the correlation induced by *U* in Fig. 6i is also of a similar block diagonal form. This correlation is purely a byproduct of the operator *U* itself, and is therefore in place before any potentially correlated (or uncorrelated) data is introduced.

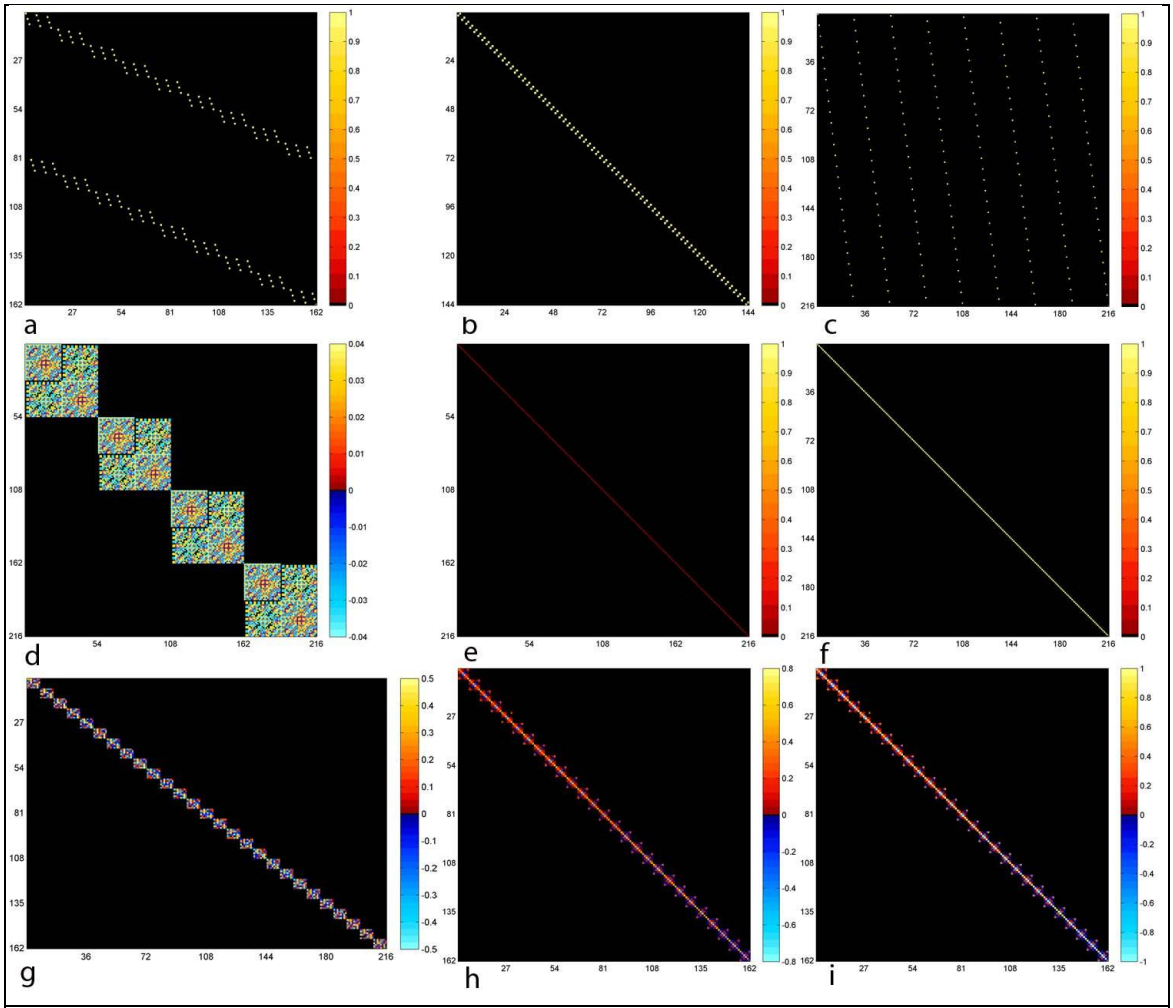

Figure 6. Operator plots used to reconstruct a 9×9 FOV from N_C=4 coils and an acceleration factor of A=3. a) Unfolding permutation, b) shift permutation, c) complex permutation, d) inverse Fourier transform operator, e) covariance induced by the inverse Fourier transform operator, f) identity correlation induced by the unfolding permutation, shift permutation, complex permutation, and inverse Fourier transform operators, g) SENSE operator, h) covariance induced by the SENSE operator, i) correlation induced by the SENSE operator..

Upon closer inspection of the correlation from *U*, the real, imaginary, and real/imaginary correlations between the center voxel and all other voxels in the reconstructed images are illustrated in Figs. 7a, 7b, and 7c with a threshold of 0.15, where the correlated voxels between folds are shown on the reconstructed magnitude image. Given that magnitude-only data has become the gold standard in image analysis, the magnitude-squared correlation about the center

voxel is illustrated in Fig. 7d. Magnitude-squared data has been chosen because it is linear in nature, and is asymptotically equivalent to magnitude-only data, which is not, and thus fits into the mathematical framework described throughout this manuscript. A mathematical derivation of the magnitude-squared covariance and correlation will not be presented in this manuscript, but can be found in Appendix B of [7]. While the correlations illustrated in Fig. 7 can be applied to any voxel in the reconstructed image, the center voxel is used throughout this manuscript for convenience.

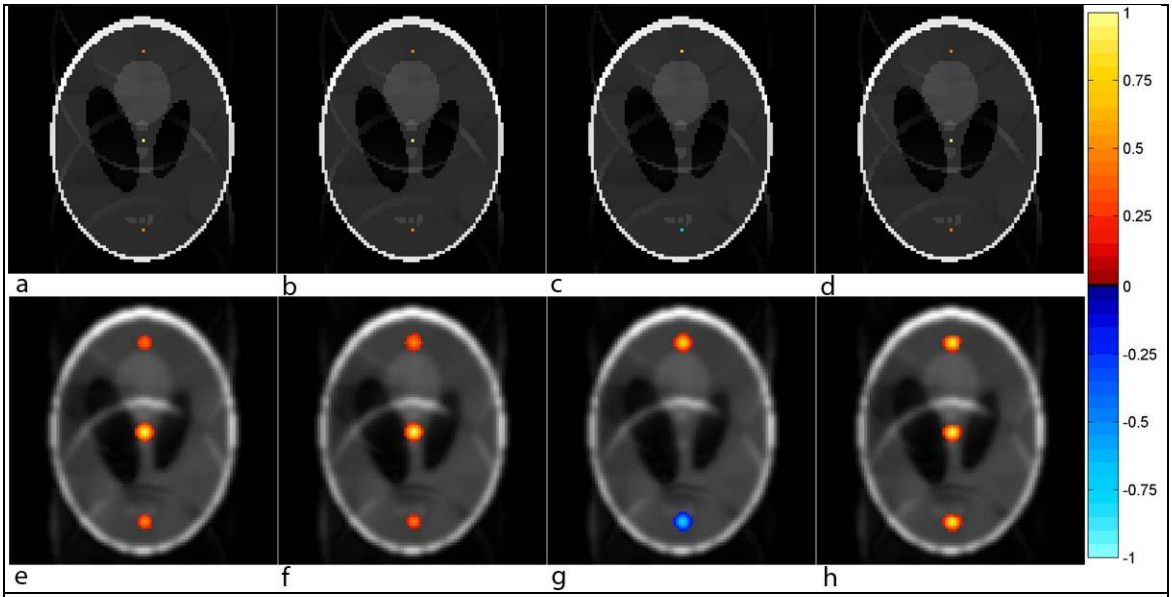

Figure 7. Induced real, imaginary, real/imaginary, and magnitude-squared voxel correlations about the center voxel by the SENSE operators with a threshold of 0.15. Smoothing was applied with a Gaussian kernel with a FWHM of 3 voxels to noiseless data, reduced in the PE direction for an acceleration factor of A=3. Correlations from operators with and without smoothing are presented with their respective magnitude underlay. a) real, b) imaginary, c) real/imaginary, d) magnitude-squared, e) smoothed real, f) smoothed imaginary, g) smoothed real/imaginary, h) smoothed magnitude-squared,

It is evident in the real, imaginary and magnitude-squared correlation images in Figs. 7a, 7b, and 7d, that there is a positive correlation induced by the SENSE reconstruction operations between the center voxel and the corresponding center voxels of the upper and lower folds. It is important to note in Fig. 7c, that while there may be no real/imaginary correlation in the center voxel itself, the SENSE unfolding operation induces a real/imaginary correlation that is positive between the center voxel and the corresponding center voxels from the upper fold, and negative

between the center voxel and the center voxel of the lower folds. The correlation induced between folds from the SENSE image reconstruction operators is further amplified if image smoothing is applied to the reconstructed [7]. Illustrated in Figs. 7e-h, one can see that the correlated voxels from each fold maintain the same sign, but are now correlated clusters of voxels instead.

As these voxels are correlated purely by the image reconstruction operators, $\Sigma = OO^{T}$, with no contribution from the theoretical phantom data itself, one would easily and mistakenly conclude that there is a correlation between voxels within the center, the anterior, and the posterior regions of the brain, in the center of each fold. This correlation could have serious implications in functional connectivitiy studies (fcMRI). These correlations exemplify the importance of considering the effects of all operators utilized in image reconstruction, particularly when those operators involve image smoothing or image combining mappings such as SENSE.

4. Experimental Application and Analysis

To observe the statistical implications of the SENSE model on experimental data, two sets of data were acquired from an array of 8 receiver coils in a 3.0 T General Electric Signa LX magnetic resonance imager. The first set of data was of a spherical agar phantom, while the second set was a series of non-task images of a human subject. Both data sets were comprised of nine 2.5 mm thick axial slices that are 96×96 in dimension for a 24 cm FOV, with the phase encoding direction oriented as anterior to posterior (top-bottom in images). Acquired for a series of 510 TRs, the data sets had a TR=1 s, TE=42.8 ms, EESP=768 ms, FA=45°, and BW = 125 kHz. The first 20 TRs were discarded to account for T_1 effects and because the echo time had been varied (in the human data), resulting in 490 TRs that were all acquired under the same conditions. All of the remaining 490 images from coils 1, 3, 5, and 7 were used in estimating both the sensitivity maps and the coil and voxel covariances, from N_C=4 equally spaced coils, to

be used in image reconstruction. Sub-sampling was simulated for an acceleration factor of A=3 by deleting lines of k-space in each of the acquired coil images in the PE direction.

Both the spherical phantom data and the human subject data were acquired with a custom Echo Planar Imaging (EPI) pulse sequence and reconstructed using locally developed image reconstruction software. The centerline of k-space for each receiver coil was acquired with three navigator echoes in order to estimate the error in the center frequency and group delay offsets between the odd and even k-space lines [7]. As EPI techniques are susceptible to dynamic fluctuations in the homogeneities of the main magnetic field, the global, temporal phase structure was corrected in both data sets after unfolding to account for field shifts associated with gradient heating and radio frequency phase variation [8].

Traditionally the raw coil sensitivity maps would be derived by normalizing the surface coil sensitivities in each voxel by the corresponding body coil sensitivities [10]. As a body coil was not available from either of the scans, the raw coil sensitivity maps were thus normalized by dividing the surface coil sensitivities by an average of the coil sensitivities in each voxel. Alternatively, a square root of the sum of squares of the coil sensitivities in each voxel could be used [10,11]. However, little difference was observed between the root sum of squares sensitivity map and the simple average used in this study. As such, the simple average sensitivity maps were used in this study as they provide both magnitude and phase images, when the root sum of squares sensitivities do not have a phase.

4.1 Phantom Data

To bridge the gap between the theoretical illustration in Section 3 and the application to the human subject data to follow, a spherical agar phantom was scanned. Unlike a human subject, the phantom is not prone to respiratory movement or physiological effects, and thus provides a good baseline for experimental observations. Coil sensitivity maps and coil

covariances were estimated from the time series of phantom images. An analysis was performed on the statistical properties of reconstructed images by observing both the estimated correlation between voxels over the course of the time series after image reconstruction as well as the correlations induced by the reconstruction operators alone.

4.1.1 Estimated Coil Covariance

In order to perform the SENSE image reconstruction process on the experimental data set, the $2N_C \times 2N_C$ real-valued isomorphism representation of the complex coil-covariance matrix was evaluated from the observed aliased voxel values. Provided with a time series of N_{TR} complex-valued, aliased, *k*-space arrays of dimension $p_x \times p_y/A$, let V denote a $p_x p_y/A \times 2N_C \times N_{TR}$ real-valued array comprised of the N_C real and N_C imaginary vectorized components of the image-space images from the N_C coils in each TR. From the 3D array V, the mean can be taken in the third dimension to estimate the mean image $\bar{V}$. Thus, the coil covariance can be estimated as

$$\hat{\Psi}_{coil} = \frac{1}{N_{TR} * rp} \sum_{t=1}^{N_{TR}} \left(V_t - \bar{V}\right)^T I_{rp}^{-1} \left(V_t - \bar{V}\right). \tag{23}$$

The estimated real-valued isomorphism representation of the $2N_C \times 2N_C$ complex coil covariance matrix, $\hat{\Psi}_{coil}$, in Eq. (23), from the time series of 490 TRs from N_C=4 receiver coils, and is listed in Table 1. Upon observation, if the estimated coil covariance, $\hat{\Psi}_{coil}$, in Table 1 is partitioned into $N_C \times N_C$ real-valued quadrants as

$$\hat{\Psi}_{coil} = \begin{bmatrix} \Psi_1 & \Psi_2 \\ \Psi_3 & \Psi_4 \end{bmatrix},$$

it can be seen that $\Psi_3 = \Psi_2^T$ and $\Psi_1 \approx \Psi_4$. To accommodate the skew-symmetric covariance structure in the SENSE model, the estimated coil covariance is reordered into

$$\Psi = \begin{bmatrix} \Psi_1 & -\Psi_4 \\ \Psi_4 & \Psi_1 \end{bmatrix},$$

replacing Ψ_2 and Ψ_3 with $-\Psi_4$ and Ψ_4 respectively.

Table 1: Coil covariances estimated from real data assuming an Identity voxel covariance

0.0863	0.0083	0.0112	0.0439	0.0013	0.0188	-0.0282	0.0149
0.0083	0.0149	0.0059	0.0184	-0.0153	0.0002	-0.0149	0.0046
0.0112	0.0059	0.0779	-0.0383	0.0186	0.0094	-0.0003	0.0403
0.0439	0.0184	-0.0383	0.1342	-0.0083	0.001	-0.0619	0.0135
0.0013	-0.0153	0.0186	-0.0083	0.0774	0.0075	0.0164	0.0296
0.0188	0.0002	0.0094	0.001	0.0075	0.0151	0.0051	0.0148
-0.0282	-0.0149	-0.0003	-0.0619	0.0164	0.0051	0.0928	-0.0379
0.0149	0.0046	0.0403	0.0135	0.0296	0.0148	-0.0379	0.1037

Table 2: Averaged coil correlation estimated from data assuming an Identity voxel covariance

1	0.0632	0.189	0.0632	0.0487	-0.0285	-0.013	-0.0285
0.0632	1	0.0632	0.189	-0.0285	0.0487	-0.0285	-0.013
0.189	0.0632	1	0.0632	-0.013	-0.0285	0.0487	-0.0285
0.0632	0.189	0.0632	1	-0.0285	-0.013	-0.0285	0.0487
0.0487	-0.0285	-0.013	-0.0285	1	0.0145	0.2155	0.0145
-0.0285	0.0487	-0.0285	-0.013	0.0145	1	0.0145	0.2155
-0.013	-0.0285	0.0487	-0.0285	0.2155	0.0145	1	0.0145
-0.0285	-0.013	-0.0285	0.0487	0.0145	0.2155	0.0145	1

To gain a better understanding of the covariance structure between coils, an average covariance was formed. This was done by taking the mean of the diagonals of each quadrant of Ψ. The main diagonal corresponds to the coil of interest, diagonals ±2 and ±4 correspond to the neighboring coils, and the third diagonal corresponds to the opposing coil for an N_C=4 array of receiver coils. This averaged covariance structure was then transformed into the correlation matrix in Table 2 by

$$\mathrm{corr}(\Psi) = D_\Psi^{-1/2} \Psi D_\Psi^{-1/2},$$

where D_Ψ is a diagonal matrix of the variances from the diagonal of Ψ, and the superscript -1/2 denotes the reciprocal of the square root of D_Ψ. Upon closer inspection of the real component of coil correlation in Table 2, one can see that the correlation between the coils along the diagonal and their neighbors loosely follows a circular Markovian structure (as used in the theoretical illustration).

4.1.2 Statistical Analysis of Phantom Data

The 490 images of the spherical phantom data set were reconstructed using the SENSE reconstruction operators assuming an identity voxel covariance structure in Eq. (19). Mean magnitude and phase images were constructed with an acceleration factor of A=3, as illustrated in Figs. 8a, and 8c. While it is not immediately evident in the mean magnitude and phase images, the standard deviation in Fig. 8e shows signs of aliasing within the phantom. In both the phase and standard deviation images in Figs. 8c and 8e, there appears to be some level of aliasing above and below the phantom. This aliasing outside of the phantom is a result of both Nyquist ghosting that has not been completely removed as well as the correlation induced between aliased voxels in the SENSE image reconstruction process.

To illustrate the effects of image smoothing, each reconstructed image in the time series of phantom data was smoothed using a Gaussian kernel with a FWHM of 3 voxels. As is expected with the implementation of a Gaussian-smoothing kernel, the magnitude in Fig. 8b has been scaled up by a factor of 4.5, correspondent with the selection of the FWHM, as illustrated in Fig. 8b. It is of note in the smoothed standard deviation in Fig. 8f that while the variance within each voxel is unchanged by the implementation of the smoothing kernel, the covariance between voxels is increased. Upon observation of the unsmoothed and smoothed standard deviation images in Fig. 8e and 8f respectively, the standard deviation within the phantom is considerably

lower than that outside, with the exception of the regions in which the aliasing occurs in the center.

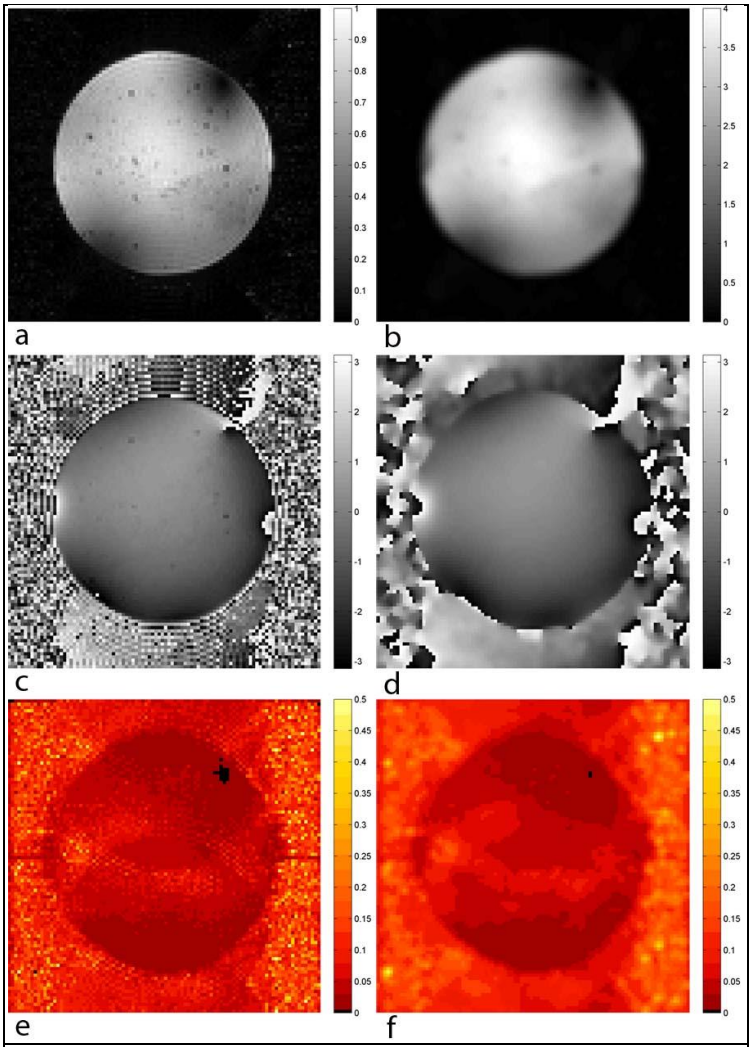

Figure 8. SENSE mean magnitude, mean phase, and standard deviation images from phantom data. Smoothing was applied with a Gaussian kernel with a FWHM of 3 voxels. a) unsmoothed magnitude, b) smoothed magnitude, c) unsmoothed phase, d) smoothed phase, e) unsmoothed standard deviation, f) smoothed standard deviation

A two-part analysis was performed on the correlations between voxels after the time series was reconstructed using the SENSE model. First, images of the correlation over the time series were constructed between the center voxel and all other voxel in the image, by reshaping the row of the overall correlation matrix corresponding to the center voxel. Second, correlation images were produced to illustrate the correlation induced by the image reconstruction operators

alone. Presented in Figs. 9a-d, with a magnitude underlay, are the real, imaginary, real/imaginary, and magnitude squared correlations between the center voxel and all other voxels in the image over the course of the time series. By comparing Figs. 9a-d with Figs. 9e-h, one can

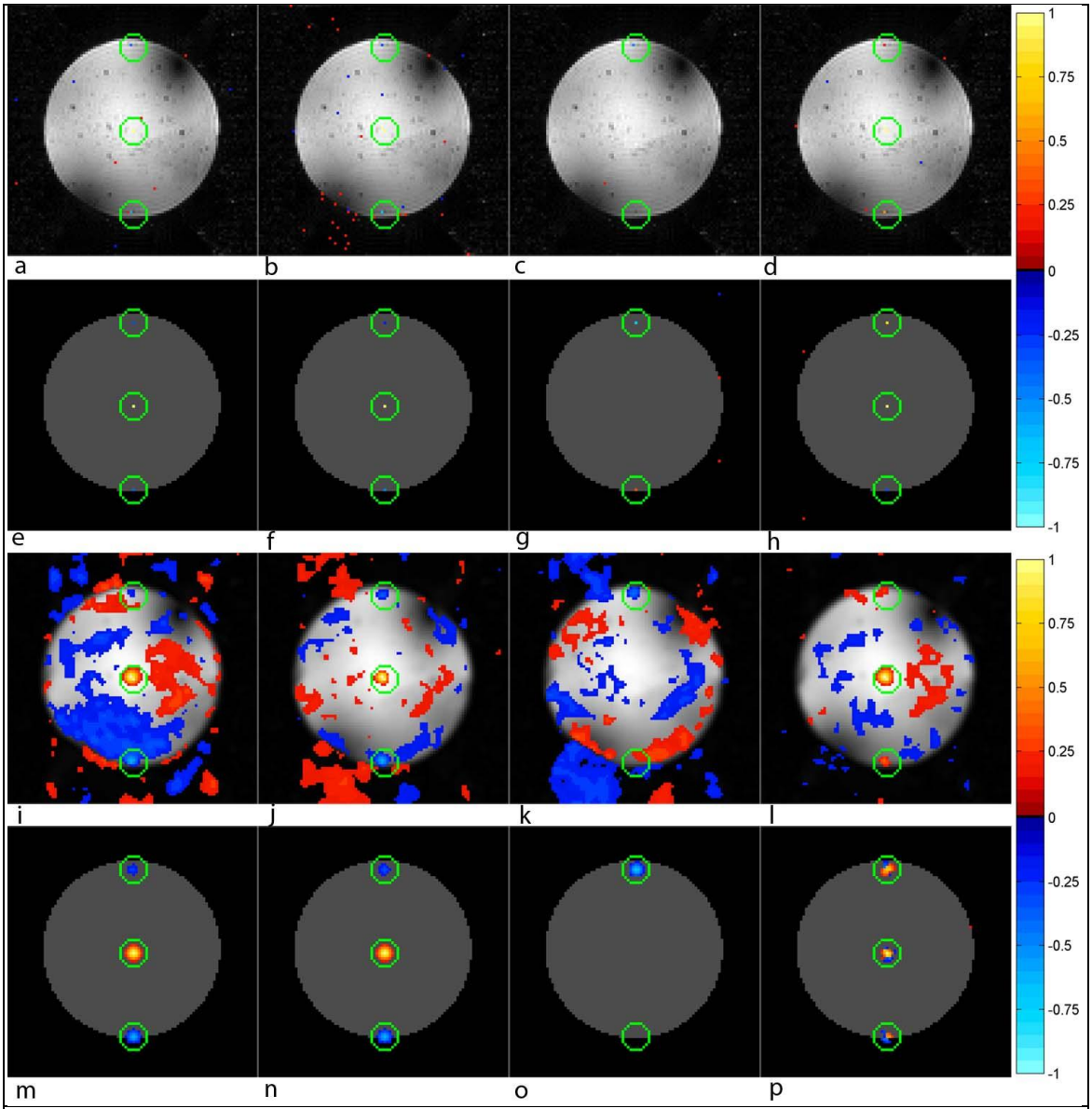

Figure 9. Estimated correlations about the center voxel throughout the time series of 490 phantom images reconstructed via the SENSE image reconstruction operators and correlations induced by the SENSE image reconstruction operators. Correlations presented with a threshold of 0.15, where estimated correlations are presented with a magnitude underlay while operator induced correlations are presented on a theoretical circular phantom. a) real estimated correlation, b) imaginary estimated correlation, c) real/imaginary estimated correlation, d) magnitude-squared estimated correlation, e) real operator induced correlation, f) imaginary operator induced correlation, g) real/imaginary operator induced correlation, h) magnitude-squared operator induced correlation, i) real estimated correlation with smoothing, j) imaginary estimated correlation with smoothing, k) real/imaginary estimated correlation with smoothing, l) magnitude-squared estimated correlation with smoothing, m) real operator induced correlation with smoothing, n) imaginary operator induced correlation with smoothing, o) real/imaginary operator induced correlation with smoothing, p) magnitude-squared operator induced correlation with smoothing.

see that there is a negative real, negative imaginary, a positive and negative real/imaginary, and a positive magnitude-squared correlation between the center voxel and the respective center voxel from the top and bottom folds. Figs. 9i-l illustrate the correlation estimated between the center voxel and all other voxels over the course of the time series with image smoothing, and Figs. 9m-p illustrate the correlations induced purely by the image reconstruction operators with image smoothing applied in image space. By comparing the real, imaginary, real/imaginary, and magnitude-squared correlations estimated over the time series in Figs. 9i-l to the operator correlations in Figs. 9m-p, it is evident that there are clusters of voxels in the center of the center, upper, and lower folds that are correlated to the center voxel. As the assumption was made that there was an identity covariance structure between voxels before image reconstruction, these correlations are therefore a byproduct of the SENSE unfolding process.

4.2 Human Subject Data

Unlike a static spherical phantom, data acquired for a human subject is prone to respiratory movement and physiological effects. Coil sensitivity maps and coil covariances were estimated from the time series of human subject images. An analysis was performed on the statistical properties of reconstructed images by observing both the estimated correlation between voxels over the course of the time series after image reconstruction as well as the correlations induced by the reconstruction operators alone.

4.2.1 Estimated Coil covariance

Following the same procedure used with the phantom data set, the $2N_C \times 2N_C$ real-valued isomorphism representation of the complex coil-covariance matrix was evaluated from the observed aliased voxel values using Eq. (23). This $2N_C \times 2N_C$ covariance was again divided into quadrants such that it could be reorganized to accommodate the skew-symmetric coil covariance

assumed by the SENSE model. The 490 images in the time series were then individually reconstructed using the SENSE image reconstruction operators, with an acceleration factor of A=3, in conjunction with the estimated coil sensitivity profiles and the estimated coil covariance structure, both with and without image smoothing.

4.2.2 Statistical Analysis of Human Subject Data

The mean magnitude and phase images, without and with smoothing, are illustrated in Figs. 10a-d. As expected, the effect of the application of the Gaussian-smoothing kernel is an increase in the mean magnitude in each voxel. A Gaussian kernel with a FWHM of 3 voxels should result in an increase in the voxel mean by a factor of 4.5, which is not the case for the human subject data set. This is most likely a result of the correction scheme utilized to account for temporal variations in the magnetic field within the brain over the course of the time series.

While aliasing was evident in the phantom standard deviation images in Figs. 8e and 8f, it is not as apparent in the standard deviation images for the human subject data in Figs. 10e and 10f. In both the phase and standard deviation images, however, there still appears to be some level of aliasing above and below the brain because of both Nyquist ghosting that has not been completely removed and the correlation induced between aliased voxels via the SENSE image reconstruction process. As image smoothing induces a correlation between voxels and their neighbors, it is to be expected that the standard deviation within a voxel will remain unchanged, while the covariance between voxels will be increased, as illustrated when comparing the standard deviation images without image smoothing in Fig. 10e to that with smoothing in Fig 10f. As was noted in the phantom data set, both the unsmoothed and smoothed standard deviations, in Figs. 10e and 10f respectively, are lower within the subject to that outside the subject.

A similar two-part analysis was performed on the correlations in the human subject data set to that in the phantom data set, where the correlations estimated throughout the time series of

human subject data between the center voxel and all other voxels in the full field-of-view reconstructed images are compared to the correlations induced by the SENSE image reconstruction operators alone. Illustrated in Figs. 11a-d, with a magnitude underlay, are the real, imaginary, real/imaginary, and magnitude squared correlations between the center voxel and all other voxels in the image over the course of the time series. In the real, imaginary and real/imaginary correlation images, there appears to be a ripple effect within the brain, which may be due to the relative quadrant in which the phase of the center voxel and other voxels reside. This is a result of phase correlations resulting from physiological effects within the human subject over the course of the time series. This can be verified by a lack of similar effect in the magnitude-squared correlation.

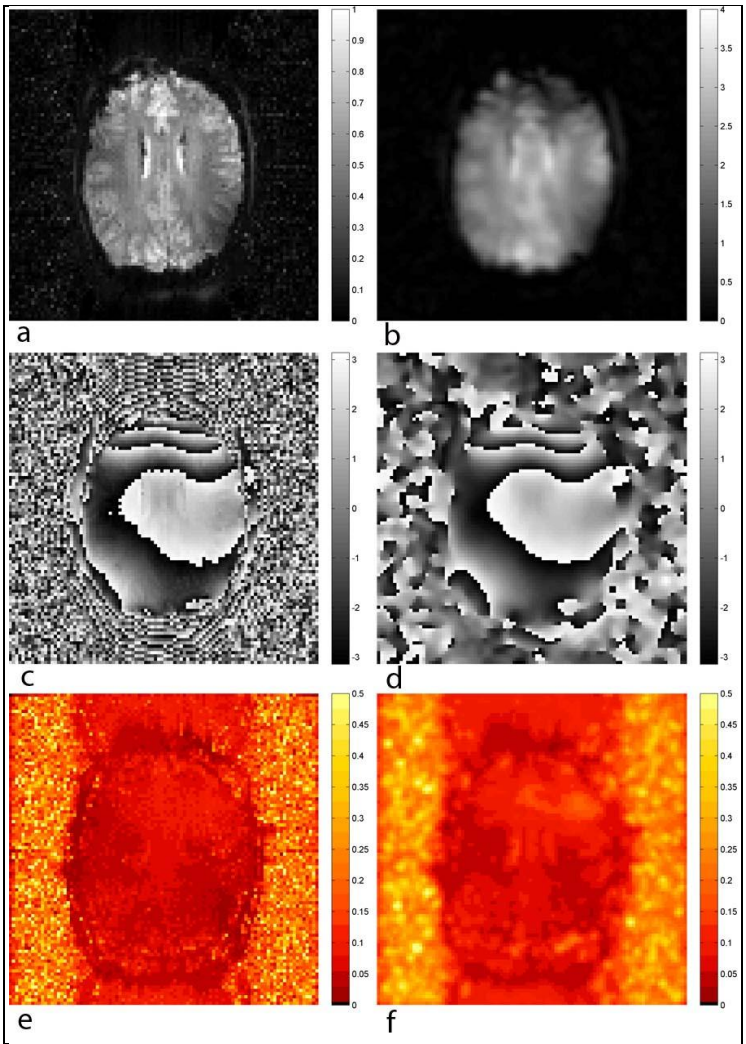

Figure 10. SENSE mean magnitude, mean phase, and standard deviation images from human subject data. Smoothing was applied with a Gaussian kernel with a FWHM of 3 voxels. a) unsmoothed magnitude, b) smoothed magnitude, c) unsmoothed phase, d) smoothed phase, e) unsmoothed standard deviation, f) smoothed standard deviation

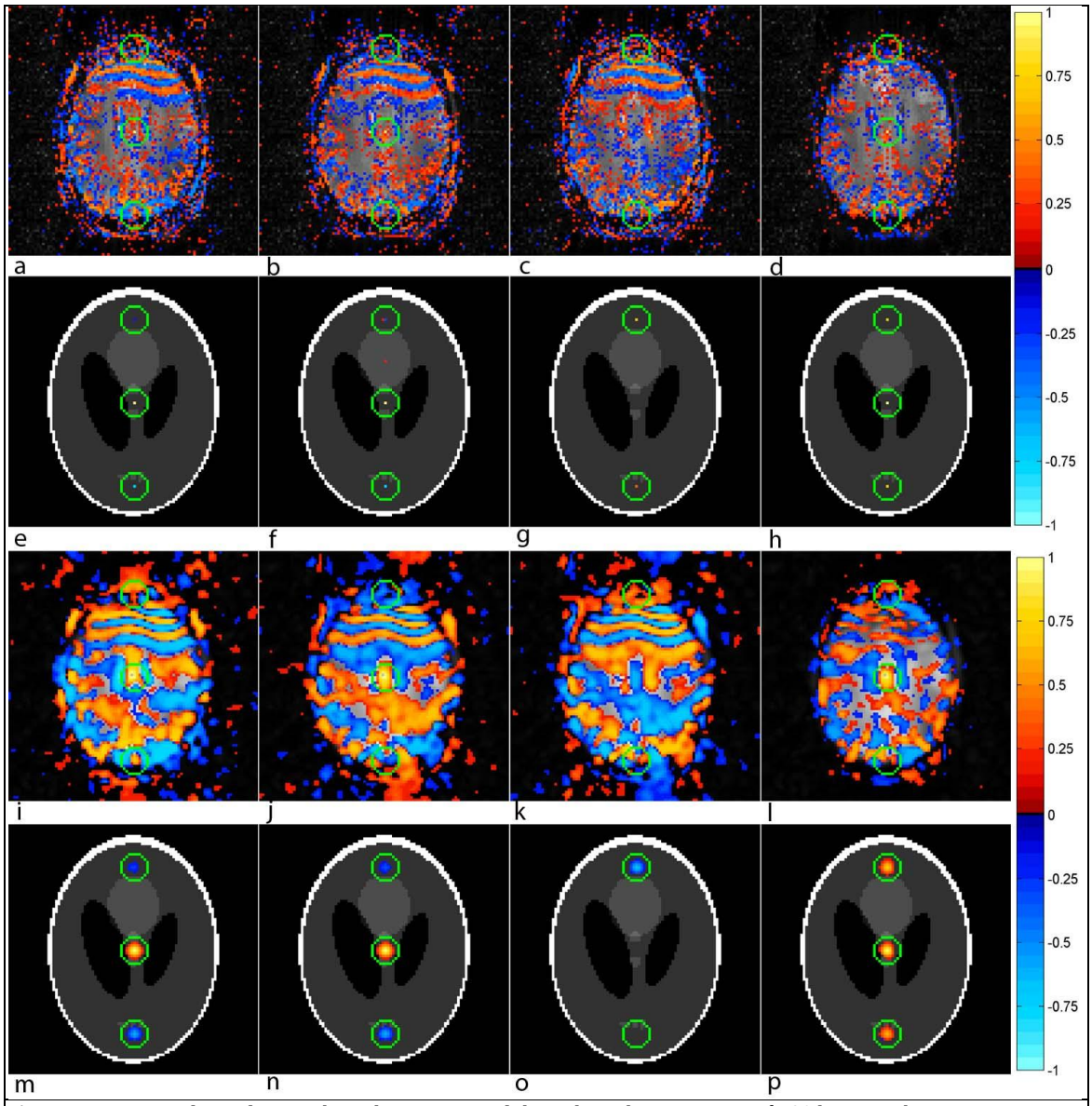

Figure 11. Estimated correlations about the center voxel throughout the time series of 490 human subject images reconstructed via the SENSE image reconstruction operators and correlations induced by the SENSE image reconstruction operators. Correlations presented with a threshold of 0.15, where estimated correlations are presented with a magnitude underlay while operator induced correlations are presented on a theoretical circular phantom. a) real estimated correlation, b) imaginary estimated correlation, c) real/imaginary estimated correlation, d) magnitude-squared estimated correlation, e) real operator induced correlation, f) imaginary operator induced correlation, g) real/imaginary operator induced correlation, h) magnitude-squared operator induced correlation, i) real estimated correlation with smoothing, j) imaginary estimated correlation with smoothing, k) real/imaginary estimated correlation with smoothing, l) magnitude-squared estimated correlation with smoothing, m) real operator induced correlation with smoothing, n) imaginary operator induced correlation with smoothing, o) real/imaginary operator induced correlation with smoothing, p) magnitude-squared operator induced correlation with smoothing.

The comparison between the correlations in Figs. 11a-d to those in Figs. 11e-h is more difficult to make than in the case of the phantom data set, as there appear to be many voxels

correlated with the center voxel in the human subject data set. In the event of image smoothing, in Figs. 11i-p, one can see that there is a positively correlated cluster of voxels about the center voxel in the real, imaginary and magnitude-squared correlation images. While there is no such correlated cluster of voxels in the center of the real/imaginary operator correlation in Fig. 11o, there appears to be a negative real/imaginary correlation in the center of the correlation estimated over the time series in Fig. 11k. It is again important to note that the SENSE model assumes an identity covariance structure between voxels before image reconstruction, and therefore any correlation estimated after the fact is a byproduct of the SENSE image reconstruction process.

5. Discussion

This work extends the mathematical framework outlined in [6,7] that allows image reconstruction operators to be expressed as matrices, and thus used to determine the statistical effects that each operator induces on the mean, covariance, and correlation of the data to be reconstructed. In this manuscript, the mathematical framework of [7] has been adapted to incorporate data that has been sub-sampled and acquired from an array of multiple receiver coils. We have provided a framework for analyzing the SENSE model as an isomorphism, allowing an analysis to be performed on the unfolding operator that is applied to the acquired data. In representing the SENSE model in terms of a real-valued isomorphism, one can see that the model assumes a skew-symmetric covariance structure between coils, as a result of the conjugate transpose utilized in the complex-valued weighted least squares estimation process. As this covariance is unlike that of real data, it was shown in the theoretical illustration of a 96×96 modified Shepp-Logan phantom that aliasing becomes apparent in both magnitude and phase images.

An investigation into the SENSE image reconstruction model for a 9×9 image showed that the three permutation matrices and inverse Fourier transform matrix are all orthogonal,

producing either an identity matrix or a scaled identity matrix when multiplied by their respective transposes. As such, there is no correlation induced by the permutations or inverse Fourier transformation. The SENSE unfolding operation, however, is a block diagonal matrix that performs a mapping from the $2N_C$ aliased voxel values from the N_C coils into $2A$ un-aliased voxel values corresponding to the A folds, and is therefore not orthogonal. It was shown in the reconstruction of a 96×96 modified Shepp-Logan phantom that the SENSE model induces a correlation between each of the previously aliased voxels in each fold. This correlation between the A un-aliased voxels becomes more severe when image smoothing is applied, resulting in correlated clusters of voxels instead.

As the SENSE model assumes an identity covariance structure between voxels before image reconstruction, any correlation observed between the previously aliased voxels is therefore altered by the unfolding process defined by the model.

This was shown for both a spherical phantom and a human subject, acquired from a 3.0 T Signa LX magnetic resonance imager. The correlation estimated about the center voxel over the course of a time series of 490 acquisitions after image reconstruction using the SENSE model showed that there was a correlation between the center voxel and the corresponding center voxel from the upper and lower folds similar to the correlations induced by the image reconstruction operators alone.

The isomorphism outlined in this manuscript, however, is very computationally intensive. In order to reconstruct a 96×96 image, with real and imaginary data, from an array of N_C=4 receiver coils that gather sub-sampled data with an acceleration factor of A=3, the operator matrix O would be 24,576×73,728. For sub-sampled data from an array of N_C=8 receiver coils, gathering sub-sampled data with an acceleration factor of A=3, the operator matrix O would be 49,152×147,456. Thus, the number of elements within the operators scales with N_C^2. This

framework can also be extended to reconstruct images in a time series with time series processing operators. However, if all operators were combined into a single operator, the number of elements would scale by the square of the number of images in the time series. Therefore, the use of sparse matrices and parallel matrix multiplication techniques, such as PUMMA [12] and SUMMA [13], would be encouraged.

Despite the high dependence on computational resources, the framework outlined in this manuscript provides an invaluable tool for analyzing the exact correlation induced by operators used in parallel image reconstruction models such as SENSE. The results indicate that operators that perform a mapping of data from multiple receiver coils to multiple folds when un-aliasing an aliased image induce a correlation between aliased voxels. Representing the image reconstruction operators as a real-valued isomorphism allows one to observe the correlation induced by all operators in each voxel of the reconstructed image. As this induced correlation is purely a result of the operators involved in reconstruction and not of any biological origin, this framework can have strong implications in functional connectivity studies. Therefore, the framework outlined in this manuscript could allow one to account for the effects each reconstruction operator has on the data in subsequent analysis.

Appendix A. Statistical Effects of Smoothing

As is common practice in fMRI, a Gaussian-smoothing kernel can be used to smooth the reconstructed images. It is important, however, to understand the effects such an operation has on the statistical properties of the data. Consider a Gaussian kernel in the center of a $2n \times 2m$ FOV with a mean of zero and a variance of σ^2

$$G(p_x, p_y) = \frac{1}{2\pi\sigma^2} e^{-\frac{(p_x^2 + p_y^2)}{2\sigma^2}} . \quad \text{(A1)}$$

It can be shown that the relationship between the FWHM, *F*, and variance of a Gaussian distribution is

$$F^2 = 2\sqrt{2\ln(2)\sigma^2},$$

and thus the Gaussian kernel in Eq. (A1) can be represented in terms of the FWHM as

$$G(p_x, p_y) = \frac{4\ln(2)}{\pi F^2} e^{-\frac{4\ln(2)(p_x^2 + p_y^2)}{\pi F^2}}. \quad \text{(A2)}$$

If one were to apply the kernel in Eq. (A2) to each voxel $j = (p_x,p_y)$ in a Cartesian grid where p_x=[-*m*:*m*], and p_y=[-*n*:*n*], with an expected value of v_j and a variance of α^2, within the reconstructed image, it would result in no change in the voxel mean,

$$E(\sum g_j \times v_j) = \sum g_j \times v_j = v_j,$$

and a change in the voxel variance as

$$\text{var}(\sum g_j \times v_j) = \sum g_j^2 \times \text{var}(v_j) = \sum g_j^2 \alpha^2.$$

In order to prevent a change in variance, it is necessary to divide all elements of the Gaussian kernel in Eq. (A2) by the square root of the sum of the squares of all elements within the kernel. This results in a scaled mean

$$E\left(\sum \frac{g_j}{\sqrt{\sum g_j^2}} \times v_j\right) = \sum \frac{g_j}{\sqrt{\sum g_j^2}} \times v_j = \frac{1}{\sqrt{\sum g_j^2}} v_j$$

and the original variance

$$\mathrm{var}\left(\sum\left(\frac{g_j}{\sqrt{\sum g_j^2}}\right)^2 \times v_j\right) = \sum \frac{g_j^{\,2}}{\sum g_j^2} \times \mathrm{var}(v_j) = \alpha^2 .$$

Therefore, the application of a Gaussian-smoothing kernel designed to leave the voxel variance unchanged has the effect of scaling the mean value within a voxel by a factor of

$$R = \frac{1}{\sqrt{\sum g_j^2}} .$$

This scaling factor *R* is directly related to the square of the FWHM, *F*, as

$$R = \frac{1}{\sqrt{\sum g_j^2}} = \left[\sum_{p_x=-m}^{m}\sum_{p_y=-n}^{n}\left(\frac{4\ln(2)}{\pi F^2} e^{-\frac{4\ln(2)(p_x^2+p_y^2)}{\pi F^2}}\right)^2\right]^{-1/2} = \frac{\pi F^2}{4\ln(2)}\left[\sum_{p_x=-m}^{m}\sum_{p_y=-n}^{n} e^{-\frac{8\ln(2)(p_x^2+p_y^2)}{\pi F^2}}\right]^{-1/2}$$

and through the linear relationship between the FWHM and the kernel variance, *R* can be shown to be linearly related to the standard deviation of the kernel, σ.

BIBLIOGRAPHY

[1] Lauterbur P.C. Image formation by induced local interactions: Examples employing nuclear magnetic resonance. Nature 1973;242, 190–191.

[2] Haacke, E.M., Brown, R., Thompson, M., Venkatesan, R. Magnetic resonance imaging: physical principles and sequence design. New York, NY, USA: John Wiley and Sons 1999.

[3] Hyde J.S., Jesmanowicz A., Froncisz W., Kneeland J.B., Grist T.M., Campagna N.F. Parallel image acquisition from noninteracting local coils. J. Magn. Reson. 1986;70, 512–517.

[4] Pruessmann, K.P., Weiger, M., Scheidegger, M.B., Boesiger, P. SENSE: Sensitivity Encoding for Fast MRI. Magn. Reson. Med. 1999;42, 952–962.

[5] Blaimer, M., Breuer, F., Muller, M., Heidemann, R.M., Griswold, M.A., Jakob, P.M. SMASH, SENSE, PILS, GRAPPA: How to choose the optimal method. Topics Magn. Reson. Imaging. 2004;15, 223–236.

[6] Rowe, D.B., Nencka, A.S., Hoffmann, R.G. Signal and noise of Fourier reconstructed fMRI data. J. Neurosci. Meth. 2007;159, 361–369.

[7] Nencka, A.S., Hahn, A.D., Rowe, D.B. A Mathematical Model for Understanding Statistical Effects of *k*-space (AMMUST-k) Preprocessing on Observed Voxel Measurements in fcMRI and fMRI, J. Neurosci. Meth. 2009;181, 268–282.

[8] Hahn, A.D., Nencka, A.S., Rowe, D.B. Improving robustness and reliability of phase-sensitive fMRI analysis using Temporal Off-resonance Alignment of Single-echo Timeseries (TOAST). NeuroImage 2009;44,742–752.

[9] Wooding, R.A. The multivariate distribution of complex normal variables. Biometrika 1956;43,212–215.

[10] Larkman, D.J., Nunes, R.G. Parallel magnetic resonance imaging. Phys Med. Biol. 2007;52,15–55.

[11] Ying, L., Liu, B., Steckner, M.C., Wu, G., Wu, M., Li, S.-J. A statistical approach to SENSE regularization with arbitrary *k*-space trajectories. Magn. Reson. Med. 2008;60, 414–421.

[12] Choi, J., Dongarra, J., Walker, D.W. PUMMA: Parallel Universal Matrix Multiplication Algorithm on distributed memory concurrent computers. Concurrency Practice and Experience 1994;6, 543–570.

[13] van de Geijn, R., Watts, J. SUMMA: Scalable Parallel Universal Matrix Multiplication Algorithm. LAPACK Working Note 99, Technical Report CS-95-286, University of Tennessee, 1995.

Marquette University

This is to certify that we have examined this copy of the thesis by

Iain P. Bruce

and have found that it is complete and satisfactory in all respects.

This thesis has been approved by:

_____

Dr. Daniel B. Rowe, Department of Mathematics, Statistics, and Computer Science

Approved on

_____